

Unsupervised Domain Adaptation with SAM-RefiSeR for Enhanced Brain Tumor Segmentation

Dillan Imans*

*Dept. of Computer Science and Engineering
Sungkyunkwan University, South Korea*

Duc-Tai Le

*Dept. of Electrical and Computer Engineering
Sungkyunkwan University, South Korea*

Phuoc-Nguyen Bui*

*Research Convergence Institute
Sungkyunkwan University, South Korea*

Hyunseung Choo†

*Dept. of Electrical and Computer Engineering
Sungkyunkwan University, South Korea*

Abstract—Robust brain-tumor segmentation in MRI must withstand domain shifts from heterogeneous scanners and protocols. Unsupervised domain adaptation (UDA) can exploit plentiful unlabeled data, yet many approaches erode boundaries, suppress tumor cues, or amplify errors from noisy pseudo-labels. General-purpose models like SAM also struggle on MRI due to the domain gap and a lack of morphology-aware consistency. We propose SAM-RefiSeR, a two-phase UDA framework that integrates SAM for reliable, annotation-efficient segmentation. Phase I reduces source-target discrepancy via Fourier-based frequency adaptation and adversarial feature alignment, aligning appearance and representations while preserving anatomy. Phase II adopts a student-teacher scheme in which SAM first refines pseudo-labels, then gates them with confidence- and morphology-aware criteria to suppress unreliable masks and curb error propagation. Across diverse cross-modality settings, SAM-RefiSeR consistently surpasses strong UDA baselines, particularly under severe shifts. By improving boundary fidelity and robustness without additional labels, SAM-RefiSeR brings brain-tumor segmentation closer to practical, generalizable clinical deployment.

Index Terms—Unsupervised domain adaptation, Image segmentation, Segment Anything Model, Frequency adaptation

I. INTRODUCTION

Deep neural networks excel in brain-tumor segmentation when train and test conditions match, but accuracy collapses under domain shift. Small variations in scanner type, field strength, or protocol can significantly alter image statistics, undermining single-domain models [1]. Annotating masks for every acquisition protocol is impractical, while unlabeled MRIs are plentiful and often shareable once de-identified. Unsupervised domain adaptation (UDA) addresses this by leveraging a labeled source domain and an unlabeled target domain to achieve domain-robust representations without additional. UDA methods fall into three categories: Pixel-level adaptation (e.g., CycleGAN [2]) aligns appearance statistics but may distort fine tumor boundaries; Feature-level alignment (e.g., ADVENT [3]) enforces domain-invariant embeddings, but can

suppress tumor-specific cues; Output-level adaptation (e.g., CBST [4]) leverages pseudo-labels but suffers from cumulative label noise. Despite enhancing cross-domain consistency, these trade-offs still limit performance.

Foundation models such as SAM [5] offer broad segmentation capacity from large-scale natural-image pretraining but struggle with the MRI domain gap, falling short of specialized medical architectures. Adapters (e.g., [6]) improve transfer but often lack morphology-aware volumetric consistency essential for reliable tumor boundaries. We propose **SAM-RefiSeR**, a two-phase UDA framework: Phase I combines adversarial and Fourier-based alignment to reduce source-target discrepancy while preserving anatomy; Phase II employs a student-teacher loop where the teacher generates prototype pseudo-labels and SAM refines/gates them via confidence and morphology tests, curbing error propagation and enabling the student to surpass SAM on delineation. The main contributions are:

- We present SAM-RefiSeR, a two-phase UDA pipeline for MRI brain-tumor segmentation that couples adversarial and frequency alignment with a SAM-guided student-teacher refinement to sharpen pseudo-labels.
- We propose a novel pseudo-label curation strategy that integrates SAM-derived confidence metrics and morphology-based selection to retain anatomically plausible masks, mitigating cumulative errors and enhancing target-domain robustness.
- Extensive experiments show SAM-RefiSeR consistently outperforming strong UDA baselines.

II. METHODS

The overall architecture of SAM-REFISER is illustrated in Fig. 1 and unfolds in two consecutive phases.

A. Phase I: Low-Frequency Adaptation with Domain Adversarial Training

Frequency adaptation [7] Each source volume x^s is paired with a randomly selected target volume x^t . Both are

*Equal contributions, †Corresponding author: choo@skku.edu

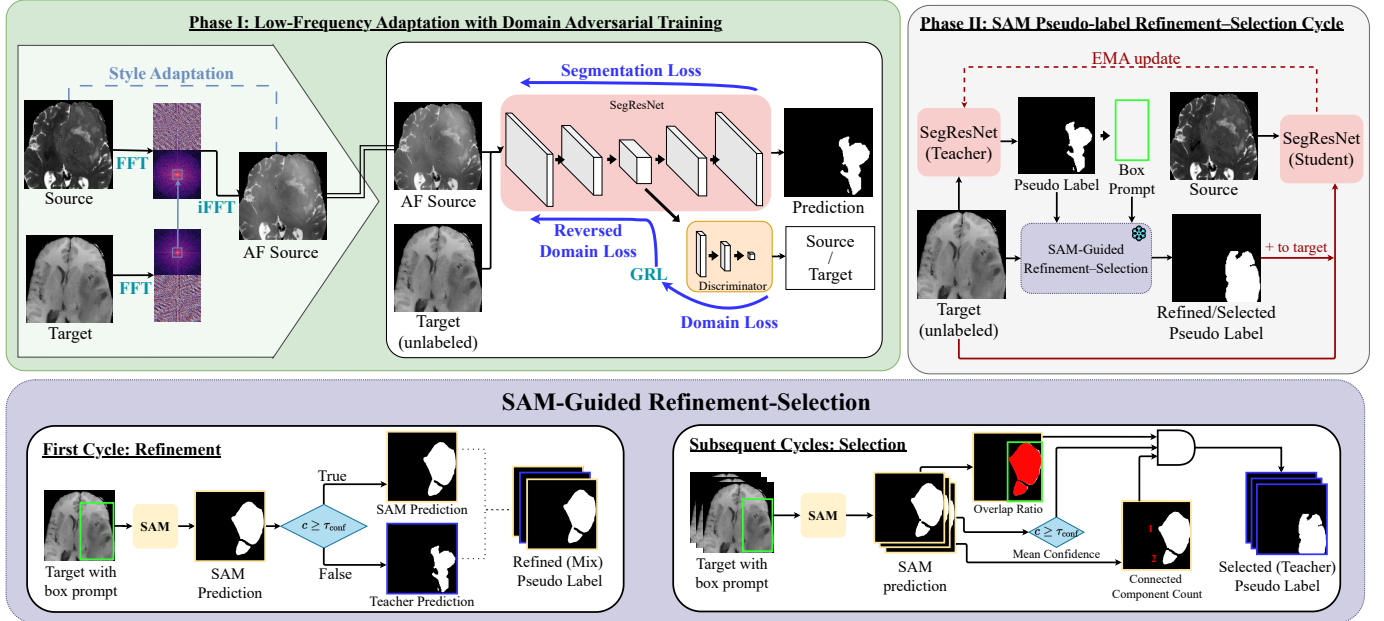


Fig. 1: Overview of the proposed 2-phase framework SAM-RefiSeR. (i)FFT, GRL, EMA, AF stand for (inverse) Fast Fourier Transform, Gradient Reversal Layer, Exponential Moving Average, and Amplitude Fused, respectively.

mapped to the spectral domain via a 3D fast Fourier transform (FFT), $\hat{x}^s = \text{FFT}(x^s)$ and $\hat{x}^t = \text{FFT}(x^t)$. All spectra are FFT-shifted so that the zero-frequency component lies at the array center. The source spectrum is factorized into amplitude and phase, $A^s = |\hat{x}^s|$ and $\Phi^s = \angle \hat{x}^s$, while only the amplitude $A^t = |\hat{x}^t|$ is retained from the target. Let $L \in (0, 1)$ be a scalar that sets the cube size and define $b = \lfloor L \min(D, H, W) \rfloor$. Empirically, $L \in [0.01, 0.03]$ works best across MRI. With the volume center at $(D/2, H/2, W/2)$, the low-frequency cube is as follows:

$$\mathcal{B} = \{(d, h, w) \mid |d - \frac{D}{2}| \leq b, |h - \frac{H}{2}| \leq b, |w - \frac{W}{2}| \leq b\}.$$

For all $(d, h, w) \in \mathcal{B}$, set $A_{d, h, w}^s \leftarrow A_{d, h, w}^t$. Swapping only low-frequency coefficients (style: intensity/contrast) while keeping high-frequency detail transfers appearance without blurring [7]. Finally, we fuse the modified amplitude $A^{s \leftarrow t}$ with the original phase Φ^s and apply an inverse FFT, $\tilde{x}^s = \text{iFFT}(A^{s \leftarrow t} e^{i\Phi^s})$, where $A^{s \leftarrow t}$ takes target amplitudes inside \mathcal{B} and source amplitudes elsewhere. The resulting volume \tilde{x}^s retains source anatomy while adopting target-style appearance.

Domain adversarial training We promote domain-invariant features using DANN [12]. Let f_θ be the segmentation encoder and g_ψ the domain discriminator predicting $d \in \{0, 1\}$ (source/target) from $z = f_\theta(x)$. The encoder and discriminator are trained adversarially via backprop to minimize the loss as follows:

$$\begin{aligned} \min_\theta \mathcal{L}_{\text{seg}}(f_\theta(x^s), y^s) + \lambda \mathcal{L}_{\text{dom}}(g_\psi(f_\theta(x)), d), \\ \min_\psi \mathcal{L}_{\text{dom}}(g_\psi(f_\theta(x)), d). \end{aligned}$$

We use soft Dice [13] on labeled source images for \mathcal{L}_{seg} and binary cross-entropy over both domains for \mathcal{L}_{dom} . Adversarial learning employs a GRL [12] between encoder f_θ and discriminator g_ψ . To avoid early instability we use a two-phase schedule: a short warm-up with $\lambda = 0$, then a logistic ramp to λ_{max} , after which λ is fixed.

$$\lambda(t) = \frac{\lambda_{\text{max}}}{1 + \exp(-\gamma(t - t_0))},$$

t is the epoch, t_0 the ramp midpoint, γ controls its steepness.

B. Phase II: SAM-Guided Pseudo-label Refinement-Selection

Using the model trained in Phase I as the teacher, we initiate iterative self-training on the unlabeled target domain.

First cycle: SAM-guided pseudo-label refinement. Let the warm-up teacher produce an initial 3D pseudo-label volume $y_i^{(0)} \in \{0, 1\}^{D \times H \times W}$ for target case i (henceforth the superscript (t) denotes the adaptation cycle: $t = 0$ for the warm-up teacher output, $t = 1$ after the present refinement step, and $t = 2, \dots, N$ for the ensuing selection cycles). Writing $y_{ij}^{(0)} \in \{0, 1\}^{H \times W}$ for its j^{th} axial slice, we compute the minimal enclosing rectangle of its foreground pixels and denote the resulting binary mask as $B_{ij} \subset \mathbb{Z}^{H \times W}$, which serves as the bounding-box prompt for SAM. We then invoke SAM on that mask B_{ij} to obtain a refined slice-mask $s_{ij}^{(1)}$ with confidence score $c_{ij}^{(1)}$. Define the slice-wise refined label as:

$$\tilde{y}_{ij}^{(1)} = \begin{cases} s_{ij}^{(1)}, & c_{ij}^{(1)} \geq \tau_{\text{conf}}, \\ y_{ij}^{(0)}, & c_{ij}^{(1)} < \tau_{\text{conf}}, \end{cases}$$

where $\tau_{\text{conf}} \in (0, 1)$ is a global confidence threshold. Thus each slice is labeled either by SAM (high-confidence case) or

by the original teacher mask. Stacking the slice-level labels yields the refined 3-D volume $\tilde{y}_i^{(1)} = \{\tilde{y}_{ij}^{(1)}\}_{j=1}^D$.

Collecting all target cases gives $\tilde{Y}^{(1)} = \{\tilde{y}_i^{(1)}\}_{i=1}^{n_t}$. We train a student model on $(X_s, Y_s) \cup (X_t, \tilde{Y}^{(1)})$ using standard segmentation loss. After each epoch, the student weights θ_S update the teacher weights θ_T via EMA:

$$\theta_T \leftarrow \alpha \theta_T + (1 - \alpha) \theta_S, \quad \alpha \in (0, 1).$$

Subsequent cycles: SAM-guided pseudo-label selection.

For each cycle $t \in \{2, \dots, N\}$ the updated teacher predicts $y_i^{(t)} \in \{0, 1\}^{D \times H \times W}$. We use SAM to obtain masks $s_{ij}^{(t)}$ and confidences $c_{ij}^{(t)}$. The SAM masks are then evaluated with three volume-level metrics; the teacher pseudo-labels are left unchanged. Let $J_i = \{j \mid B_{ij} \text{ exists}\}$ be the slice indices, and write $|\cdot|$ for the number of foreground voxels in a binary mask.

- 1) Mean confidence $\bar{c}_i^{(t)} = \frac{1}{|J_i|} \sum_{j \in J_i} c_{ij}^{(t)}$. High $\bar{c}_i^{(t)}$ signals strong epistemic certainty in SAM's slice-wise proposals, whereas low values often coincide with weak edges or out-of-plane artifacts.
- 2) Overlap ratio $o_i^{(t)} = \frac{\sum_{j \in J_i} |s_{ij}^{(t)}|}{\sum_{j \in J_i} |B_{ij}|}$, where $|B_{ij}|$ is the number of pixels in the bounding box. Very small ratios flag masks dominated by false positives; ratios near 1 indicate overly loose boxes capturing non-tumor tissue; intermediate values typically correspond to well-focused, accurate segmentation.
- 3) Connected-component $n_i^{(t)} = \text{CC}(\text{Stack}\{s_{ij}^{(t)}\}_{j \in J_i})$, counts connected foreground components in 3D masks formed by stacking all predictions. Masks with a small

handful of components are plausible, whereas many tiny components indicate noise or over-segmentation.

A volume is retained iff:

$$\bar{c}_i^{(t)} \geq \tau_{\text{conf}} \wedge o_i^{(t)} \in [\tau_{\text{overlap}}^-, \tau_{\text{overlap}}^+] \wedge n_i^{(t)} \leq \tau_{\text{cc}}.$$

III. EXPERIMENTS AND RESULTS

A. Dataset and Implementation Details

We use the BraTS 2021 multimodal MRI dataset [14] with voxel labels for ET (Enhancing Tumor), TC (Tumor Core), and WT (Whole Tumor). We perform a patient-wise 80/20 train/test split. We crop all images to the nonzero region, to $128 \times 128 \times 128$, and apply per-volume min-max normalization. Experiments use PyTorch on two NVIDIA RTX 2080 Ti. Phase I trains for 150 epochs with Adam ($\text{lr} = 10^{-4}$). Phase II comprises five student-teacher self-training cycles. The teacher is updated by EMA with decay $\alpha = 0.99$. Refinement/selection thresholds are chosen via grid search on a small unlabeled target subset: $\tau_{\text{conf}} \in \{0.5, 0.6, \dots, 0.9\}$ for both phases; for selection we additionally sweep $\tau_{\text{overlap}}^- \in \{0.3, 0.4, 0.5\}$, $\tau_{\text{overlap}}^+ \in \{0.6, 0.7, 0.8\}$ with $\tau_{\text{overlap}}^- < \tau_{\text{overlap}}^+$, and component caps $\tau_{\text{cc}} \in \{1, 3, 5, 10, 20, 30, 50\}$.

B. Comparison with Existing Methods

Tables I (a,b) report results using T1CE and T2 as source domains, comparing SAM-RefiSeR with SegResNet [15] and four UDA baselines. Averaged over ET/TC/WT, SAM-RefiSeR achieves the highest Dice and lowest HD95 in both settings. Notably, SAM-RefiSeR shows the largest improvements under severe domain shifts, such as in T1CE \rightarrow T2 (Dice

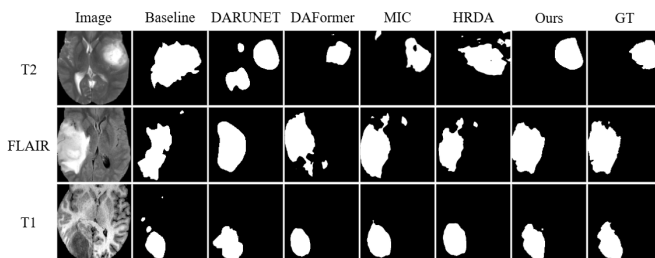
TABLE I: Comparison of methods across imaging modalities: T1CE as source (left) and T2 as source (right).
 \uparrow : higher is better; \downarrow : lower is better.

(a) T1CE as source

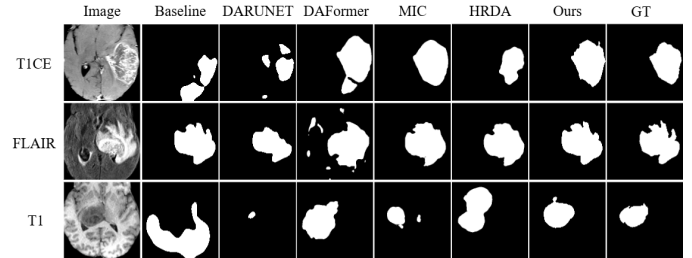
Method	T2		FLAIR		T1	
	Dice \uparrow	HD95 \downarrow	Dice \uparrow	HD95 \downarrow	Dice \uparrow	HD95 \downarrow
Baseline	7.6	76.4	28.9	71.3	19.9	59.7
DAR-UNET [8]	35.5	57.1	43.2	40.3	26.3	51.1
DAFormer [9]	41.0	43.3	50.4	27.2	49.8	25.3
MIC [10]	45.2	39.2	49.3	28.3	49.4	24.3
HRDA [11]	34.4	49.5	51.1	26.1	49.4	26.0
Ours	54.2	25.3	58.5	19.6	57.1	23.2

(b) T2 as source

Method	T1CE		FLAIR		T1	
	Dice \uparrow	HD95 \downarrow	Dice \uparrow	HD95 \downarrow	Dice \uparrow	HD95 \downarrow
Baseline	8.5	64.5	55.6	23.6	4.7	80.2
DAR-UNET [8]	34.9	51.8	45.4	31.2	15.8	76.3
DAFormer [9]	48.0	40.3	59.8	20.6	45.6	34.3
MIC [10]	52.6	36.0	60.8	20.2	40.7	37.3
HRDA [11]	52.9	27.7	62.8	19.3	43.5	29.3
Ours	60.9	23.5	64.4	16.3	50.2	24.6



(a) Model trained on T1CE.



(b) Model trained on T2.

Fig. 2: Qualitative comparison of methods with T1CE and T2 as source domains.

54.2%, HD95 25.3 voxels). Improvements persist but narrow in visually closer domains (e.g., T2→FLAIR). Figures 2 (a,b) visually demonstrate fewer false positives aligning with the quantitative results, where SAM-RefiSeR accurately delineates subtle tumor structures missed by other methods.

C. Ablation Studies

Table II ablates Phase I and Phase II. Phase I provides initial improvements in Dice and HD95, while Phase II delivers the most significant gains, further enhancing performance. Table III, which ablates the number of cycles, shows that most gains arrive by cycle 3. Thus, early cycles deliver the bulk of improvement; later cycles offer modest polish.

TABLE II: Ablation study of model stages from the T1CE- and T2-source domains to different MRI modalities.

(a) T1CE as source						
Method	T2		FLAIR		T1	
	Dice↑	HD95↓	Dice↑	HD95↓	Dice↑	HD95↓
Baseline	7.6	76.4	28.9	71.3	19.9	59.7
Phase I	14.6	62.7	37.5	42.0	30.1	42.8
Ours	54.2	25.3	58.5	19.6	57.1	23.2
(b) T2 as source						
Method	T1CE		FLAIR		T1	
	Dice↑	HD95↓	Dice↑	HD95↓	Dice↑	HD95↓
Baseline	8.5	64.5	55.6	23.6	4.7	80.2
Phase I	27.1	43.5	58.1	19.5	19.5	73.7
Ours	60.9	23.5	64.4	16.3	50.2	24.6

TABLE III: Ablation study of cycle-wise performance from the T1CE- and T2-source domains to different MRI modalities.

(a) T1CE as source						
Cycle	T2		FLAIR		T1	
	Dice↑	HD95↓	Dice↑	HD95↓	Dice↑	HD95↓
1	34.7	49.7	46.1	34.2	53.1	28.5
3	47.3	30.7	55.1	20.7	56.0	26.5
5	54.2	25.3	58.5	19.6	57.1	23.2
(b) T2 as source						
Cycle	T1CE		FLAIR		T1	
	Dice↑	HD95↓	Dice↑	HD95↓	Dice↑	HD95↓
1	51.9	39.2	62.4	19.5	33.0	39.0
3	55.8	35.9	63.2	16.5	48.4	25.1
5	60.9	23.5	64.4	16.3	50.2	24.6

IV. CONCLUSION

SAM-RefiSeR delivers a robust, two-phase solution to unsupervised domain adaptation for brain-tumor segmentation. The first phase combines Fourier-based frequency adaptation with adversarial training to bridge source–target gaps while preserving anatomical detail. The second phase employs an iterative student–teacher framework, where SAM refines and filters pseudo-labels through confidence and morphology checks, halting error propagation and steadily improving

target-domain performance. SAM-RefiSeR consistently outperforms prior UDA baselines across modality shifts, with the largest margins under the most severe cross-modality gaps. Future work will extend evaluations to diverse datasets to validate generalizability and robustness.

ACKNOWLEDGEMENT

This work was supported in part by IITP grant funded by the Korean government (MSIT) under IITP-2025-RS-2020-II201821 (30%), RS-2024-00459512 (30%), RS-2021-II212068 (20%), and RS-2019-III190421 (20%).

REFERENCES

- [1] P.-N. Bui, D.-T. Le, J. Bum, S. Kim, S. J. Song, and H. Choo, “Semi-supervised learning with fact-forcing for medical image segmentation,” *IEEE Access*, vol. 11, pp. 99 413–99 425, 2023.
- [2] J.-Y. Zhu, T. Park, P. Isola, and A. A. Efros, “Unpaired image-to-image translation using cycle-consistent adversarial networks,” in *Proceedings of the IEEE international conference on computer vision*, 2017, pp. 2223–2232.
- [3] T.-H. Vu, H. Jain, M. Bucher, M. Cord, and P. Pérez, “Advent: Adversarial entropy minimization for domain adaptation in semantic segmentation,” in *Proceedings of the IEEE/CVF conference on computer vision and pattern recognition*, 2019, pp. 2517–2526.
- [4] Y. Zou, Z. Yu, B. Kumar, and J. Wang, “Unsupervised domain adaptation for semantic segmentation via class-balanced self-training,” in *Proceedings of the European conference on computer vision (ECCV)*, 2018, pp. 289–305.
- [5] A. Kirillov, E. Mintun, N. Ravi, H. Mao, C. Rolland, L. Gustafson, T. Xiao, S. Whitehead, A. C. Berg, W.-Y. Lo *et al.*, “Segment anything,” in *Proceedings of the IEEE/CVF international conference on computer vision*, 2023, pp. 4015–4026.
- [6] T. Chen, L. Zhu, C. Ding, R. Cao, S. Zhang, Y. Wang, Z. Li, L. Sun, P. Mao, and Y. Zang, “Sam fails to segment anything?—sam-adapter: Adapting sam in underperformed scenes: Camouflage, shadow, and more,” *arXiv preprint arXiv:2304.09148*, vol. 2, no. 5, p. 7, 2023.
- [7] Y. Yang and S. Soatto, “Fda: Fourier domain adaptation for semantic segmentation,” in *Proceedings of the IEEE/CVF conference on computer vision and pattern recognition*, 2020, pp. 4085–4095.
- [8] K. Yao, Z. Su, K. Huang, X. Yang, J. Sun, A. Hussain, and F. Coenen, “A novel 3d unsupervised domain adaptation framework for cross-modality medical image segmentation,” *IEEE Journal of Biomedical and Health Informatics*, 2022.
- [9] L. Hoyer, D. Dai, and L. Van Gool, “DAFormer: Improving network architectures and training strategies for domain-adaptive semantic segmentation,” in *Proceedings of the IEEE/CVF Conference on Computer Vision and Pattern Recognition (CVPR)*, 2022, pp. 9924–9935.
- [10] L. Hoyer, D. Dai, H. Wang, and L. Van Gool, “MIC: Masked image consistency for context-enhanced domain adaptation,” in *Proceedings of the IEEE/CVF Conference on Computer Vision and Pattern Recognition (CVPR)*, 2023.
- [11] L. Hoyer, D. Dai, and L. Van Gool, “HRDA: Context-aware high-resolution domain-adaptive semantic segmentation,” in *Proceedings of the European Conference on Computer Vision (ECCV)*, 2022, pp. 372–391.
- [12] Y. Ganin, E. Ustinova, H. Ajakan, P. Germain, H. Larochelle, F. Laviolette, M. March, and V. Lempitsky, “Domain-adversarial training of neural networks,” *Journal of machine learning research*, vol. 17, no. 59, pp. 1–35, 2016.
- [13] F. Milletari, N. Navab, and S.-A. Ahmadi, “V-net: Fully convolutional neural networks for volumetric medical image segmentation,” in *2016 fourth international conference on 3D vision (3DV)*. Ieee, 2016, pp. 565–571.
- [14] B. H. Menze, A. Jakab, S. Bauer, J. Kalpathy-Cramer, K. Farahani, J. Kirby, Y. Burren, N. Porz, J. Slotboom, R. Wiest *et al.*, “The multimodal brain tumor image segmentation benchmark (brats),” *IEEE transactions on medical imaging*, vol. 34, no. 10, pp. 1993–2024, 2014.
- [15] A. Myronenko, “3d mri brain tumor segmentation using autoencoder regularization,” in *International MICCAI brainlesion workshop*. Springer, 2018, pp. 311–320.